


Contents

Table of Contents	i
List of Tables	i
1 Coupling of Nanodiamonds to Photonic Structures	1
1.1 Additional Experimental Methods	2
1.1.1 Nanomanipulator	3
1.1.2 Determination of The Position of Nanodiamonds	3
1.1.3 The Pick-And-Place Process	7
1.2 VCSELs	8
1.2.1 Vertical-Cavity Surface Emitting Laser Structure	8
1.2.2 SiV center in a Vertical-Cavity Surface Emitting Laser	10
1.3 Antennas	14
1.3.1 Plasmonic Antennas	15
1.3.2 Plasmonic Antenna Design	17
1.3.3 SiV center in a Plasmonic Double Bowtie Antenna	20
Index	27

List of Tables

Chapter 1

Coupling of Nanodiamonds to Photonic Structures

In the previous chapter, we reported on photoluminescence properties of different sets of SiV centers. Across the available samples, emitters were found to exhibit considerable variations in wavelength, linewidth as well as intensity of zero-phonon-lines. This broad variety in combination with the ability to examine SiV centers individually opens up the possibility to preselect emitters according to desired spectroscopic parameters, such as narrow linewidths, high countrates and single photon emission.

Once suitable emitters are identified, their host nanodiamonds can be moved with precision using pick-and-place methods. In particular, SiV centers may be transferred and coupled to photonic structures where their extraordinary properties can be exploited to create single photon source. Such sources are useful tools, widely required for applications in metrology and various quantum technologies such as quantum computing or quantum cryptography.

In the scope of this thesis, nanodiamonds including suitable SiV centers were identified and coupled to two different kinds of structures: Vertical-Cavity Surface Emitting Lasers (VCSELs) and plasmonic nanoantennas.

To create a hybrid-integrated single photon source, a nanodiamond containing an SiV center placed on top of a VCSEL. The SiV center is positioned such that it is directly pumped by the VCSEL output laser beam. Thus, the emission of the SiV center is steered indirectly via the operation of the VCSEL. Through the use of suitable optical filters allowing only SiV center fluorescence light to emerge, a controlled single photon source can be realized. This system is interesting in the context of metrological applications, as it constitutes a promising building block for a portable device ready to calibrate single photon detectors.

Coupling SiV centers to plasmonic nanoantennas aims at enhancing the detectable photoluminescence intensity of an emitter. As described in previous chapters, not only ZPL position and linewidth, but also the photoluminescence intensity varies strongly among individual SiV centers. Obtaining a single photon source with a photon flux rate large enough to reliably and precisely be measured by a low photon flux detector is a key requirement for applications in metrology [?]. Furthermore, plasmonic antennas can be used to tune the emitters' photoluminescence spectrum.

ich
glaub,
das ist
bullshit

der satz
muss
noch ein-
massiert
werden

1.1 Additional Experimental Methods

Coupling SiV centers to photonic structures requires specialized experimental methods. A range of challenges must be overcome: First, additionally to the spectroscopic pre-selection, the pick-and-place process poses further technical restrictions on the suitability of a host nanodiamond. The size of the host nanodiamond has to be bigger than 70 nm and they have to lie isolated on the substrate surface, i.e. with a distance of about one micrometer. This substantially reduces the number of SiV center candidates ready to be coupled to photonic structures. Another challenge is posed by accurately picking up a single nanodiamond hosting an SiV center and placing it precisely at a specified position within a given photonic structure. Furthermore, since the SiV center is to function as the photoluminescence emitter, it must not be damaged during the relocation process. To minimize both the damage cause by electron radiation, both the dose and the energy are minimized. Hence, the pick-and-place process is performed as fast as possible and with a low acceleration voltage that is just strong enough to see a hazy image of the nanodiamond.

In the context of this thesis we explored the following methods to couple nanodiamonds to photonic structures:

1. Directly spin-coat the target structures with a nanodiamond solution and consecutively look for a structure containing a nanodiamond with an SiV center exhibiting the desired spectroscopic properties. Frankly, this method relies on chance and is only feasible for the application with antenna structures due to the large number of antennas on one substrate. It is not advised to be used with VCSELs because of their morphology and the small number of VCSELs on an individual piece of substrate.
2. Identify nanodiamonds containing suitable SiV centers and individually relocate them to the destination structure using the tip in a scanning electron microscopy to perform a pick-and-place routine. For this method to be effective, nanodiamonds must have a certain size. The obvious advantage of this method is the fact that only the very best emitters are used. Furthermore, the pick-and-place process can be monitored in realtime. On the other hand, the electron radiation present during the pick-and-place process may damage the SiV center, introducing a risk of completely invalidating an emitter.
3. Identify nanodiamonds containing suitable SiV centers and individually relocate them to the destination structure using an atomic force microscope to perform a pick-and-place routine. While this method has the advantage that the nanodiamonds are not irradiated with electrons, the disadvantage is that it is not possible to observe the picking process in real time. As a consequence, the area of the preselected nanodiamond has to be scanned after every pick-up attempt, which is prohibitively time consuming and therefore was not further pursued after initial trials.

In the following we detail the pick-and-place technique since it the key technique in this chapter. We also discuss the properties of the nanomanipulator and how we identify nanodiamonds suitable for pick-and-place transfer. The pick-and-place process itself is very fickle and difficult to execute correctly. We are grateful for the guidance and support provided by C. Pauly, group of F. Mücklich, Saarland University in addition to the nanomanipulator setup itself.

1.1.1 Nanomanipulator

The nanomanipulator used for our experiments (Kleindiek, model MM3A-EM) has a exchangeable tungsten tip mounted inside a Thermo Scientific™ Helios NanoLab™ DualBeam™ microscope. This device combines a focussed ion beam and an electron microscope. The bent nanomanipulator tip can be seen in Figure ?? has 3 degrees of freedom: up/down and left/right both in an arc up to 240°, and 12 mm in/out.

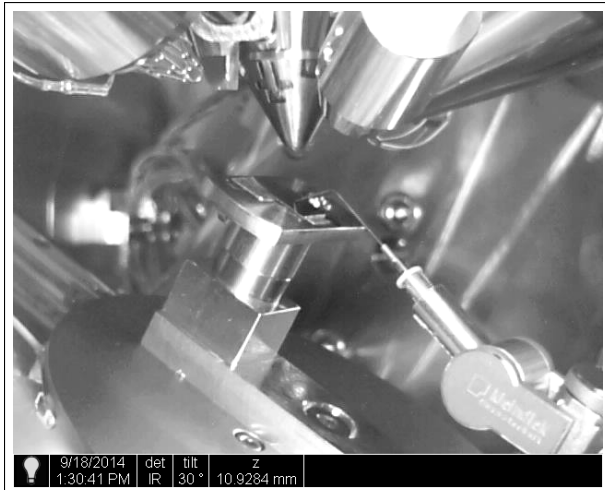


Figure 1.1: Image of the nanomanipulator mounted in the FIB. The arrows indicate the degrees of freedom of motion of the nanomanipulator. The custom made workbench is situated in the middle of the picture. On top of it, there is a 1 cm² substrate with coated nanodiamonds, the nanomanipulator tip pointing to the middle of it. Behind it, there is the target vertical-cavity surface emitting laser. Perpendicular to the workbench, the objective of the electron microscope can be seen. The angled cone perpendicular to the top edge of the image is the objective of the focussed ion beam.

Before using the nanomanipulator, its tip was “sharpened” with a focussed ion beam by etching away tungsten with gallium ions. Its final radius of curvature amounts to 100 nm. The sharpening enables the pick-up of nanodiamonds of a size suitable for use with photonic structures. In Figure 1.2a two sharpened tips are shown.

1.1.2 Determination of The Position of Nanodiamonds

Using the confocal setup detailed in ?? we identified nanodiamonds containing SiV centers suitable for the use in photonic structures. However, to actually move those nanodiamonds to a target photonic structure the SEM setup described in the previous section must be used. This implies that after substrates containing suitable nanodiamonds are mounted in the SEM setup, the same nanodiamonds must be located on the substrate in order for the nanomanipulator to address them correctly. To facilitate this and help locate relevant nanodiamonds, 10 µm² cross markers with a nominal depth of 40 nm were milled into the iridium coating of the silicon substrate using the focussed ion beam prior to spin-coating the substrate with nanodiamond solution. The markers were arranged in a regular 11 × 11 grid covering an area of 0.5 mm ×

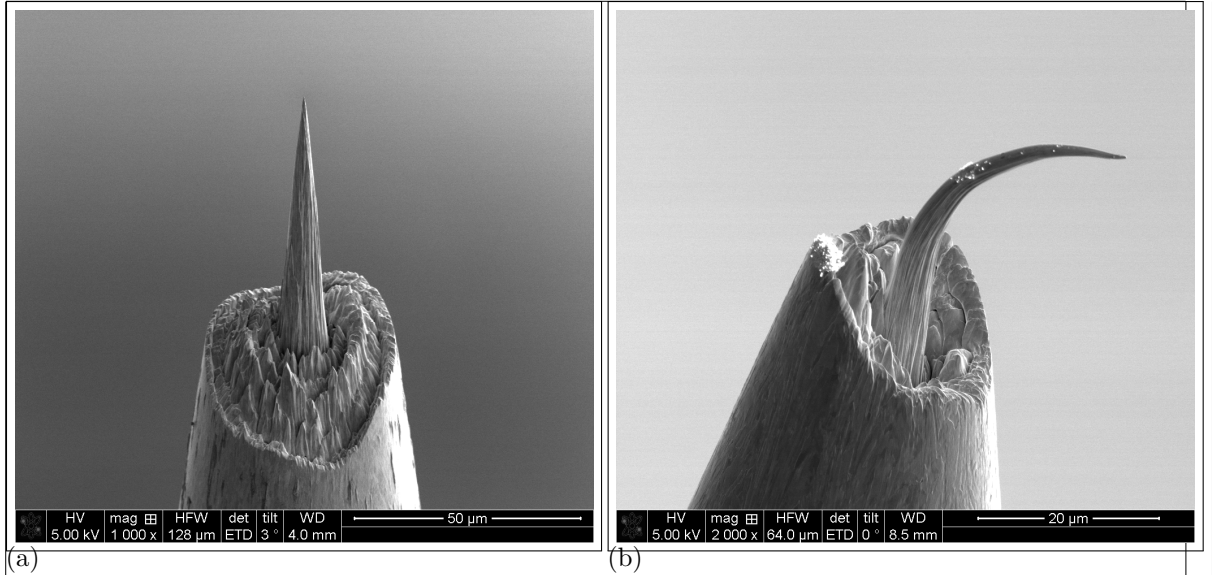


Figure 1.2: Detail of tips used as nanomanipulators. The actual tip can be seen projecting out from a bigger supporting structure. (a) Well-formed tip after sharpening. (b) Bend tip, silently attesting to the use of excessive force.

0.5 mm. Figure 1.3a illustrates a sample array. Typically three arrays of markers were milled per substrate used.

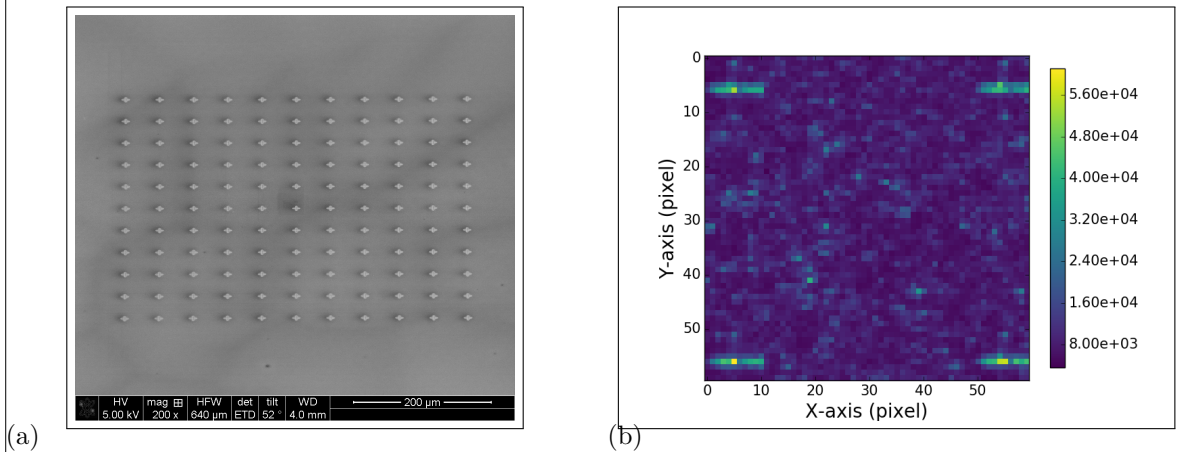


Figure 1.3: (a) Top-view of a regular array of cross markers. (b) White light scan of an area. Cross markers can be seen in all four corners.

To record the position of a nanodiamond with respect to a cross marker, we used two different methods:

In the first method the confocal setup is used with a white light source illuminates the sample from the side at an acute angle. As a result, the edges of the cross markers become visible in the fluorescence light scan, see Figure 1.3b. After turning the white light lamp off, the same area is scanned again to record the fluorescence from the SiV centers. An overlay of the two images identifies the position of fluorescent SiV centers with respect to the cross markers.

The disadvantage of this method is the increased time consumption, as every scan for every subregion of the sample has to be performed twice. As only fluorescence light scans are performed, no information about the size of individual nanodiamonds is available. Furthermore, it remains unknown whether nanodiamonds are present in isolation or close to each other. Such information is only available in the SEM where the pick-and-place is conducted. It is only at this later stage, that individual nanodiamonds can be excluded as unusable for the pick-and-place process. For such nanodiamonds the time spend of characterizing its properties was unfortunately wasted.

To mitigate this problem, a more efficient method consists of scanning the substrate first using a commercial laser scanning microscope. The laser scanning microscope is a confocal microscope where the focus of a laser can be used to obtain the height of a structure. When scanning an array of cross markers a greyscale image is obtained, where the grey value corresponds to the height deviation of a structure. As a result, both the crosses with a nominal depth of 40 nm and the nanodiamonds themselves are revealed as darker shades of grey. In contrast to the previous method, information on the size and isolation of nanodiamonds is accessible. After scanning the substrate with the laser scanning microscope, it is inserted into the confocal setup. While observing the surface with a CCD camera, a specific cross marker is chosen as the starting point for a fluorescence light scan. Comparing the laser scanning microscope image and a fluorescence light scan, fluorescent dots of the fluorescence light scan can be attributed to nanodiamonds in the laser scanning microscope scan. ?? illustrate the process.

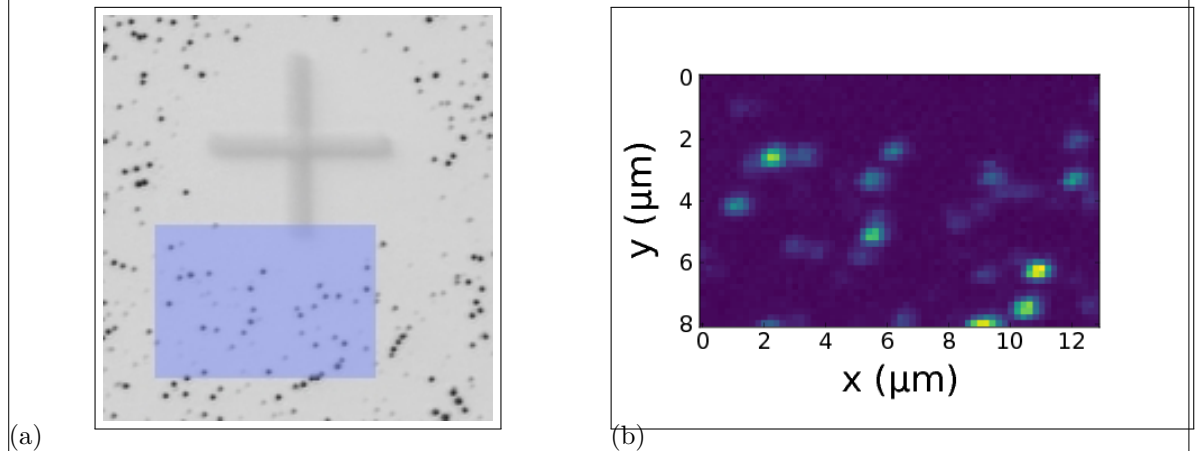


Figure 1.4: a) Picture recorded with a commercial high resolution laser scanning microscope. Cross marker is visible as well. b) Photoluminescence scan of a $8 \mu\text{m} \times 13 \mu\text{m}$ corresponding to the blue shaded area in b). The area shaded in blue represents the photoluminescence scan in image b).

<<< HEAD

An nanodiamond pre-characterized in the confocal setup exhibiting the preferred spectroscopic properties has to be found again in the SEM setup where the nanomanipulator is installed. Therefore, we milled cross markers into the iridium coating of the silicon substrate using the focussed ion beam prior to spin-coating the substrate with nanodiamond solution. The crosses' size is $10 \times 10 \mu\text{m}^2$ are exhibit a nominal depth of 40 nm. Four crosses are the cornerpoints of a $50 \times 50 \mu\text{m}^2$ square. The 10×10 crosses spaned one field of crosses; we usually put 3 fields of

fib pa-
rameter

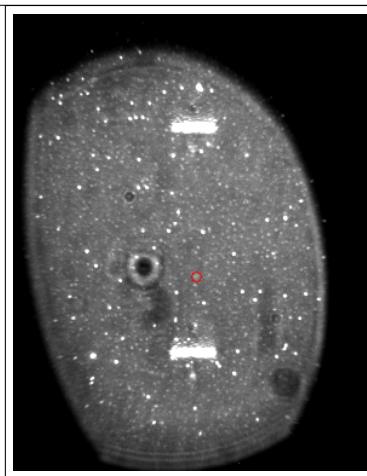


Figure 1.5: Image of the sample surface of 100 nm wet-milled nanodiamonds spin-coated on an iridium substrate illuminated with diffuse white light. The white bars are the horizontal bars of the cross markers which serve as a coarse orientation on the sample surface, the white dots are nanodiamonds, the big black spot is an artifact.

crosses on one substrate.

To record the position of a nanodiamond with respect to a cross marker, we used two different methods:

- Scanning the sample in the confocal setup while a white light source illuminates the sample from the side in an acute angle. The edges of the cross markers are visible in the fluorescence scan. After turning the white light lamp off, the same area is scanned once more to record the fluorescence from the SiV centers. An overlay of the two images identifies the position of fluorescent SiV centers with respect to the cross markers. The disadvantage of this method is, that it takes a lot of time, as every scan has to be performed twice. Also, as only fluorescence light scans are performed, no information of the nanodiamonds is accessible. Such information comprises of the size of the individual nanodiamonds and whether the nanodiamonds lie isolated on the substrate surface. These parameters are only available during the pick-and-place process in the SEM. An emitter with optimal optical properties can turn out not to be suited for pick-and-place just before the process itself, hence the time spent to optically characterize an emitter was in vain.
- A more efficient method is scanning the substrate first in a commercial laser scanning microscope . The laser scanning microscope is a confocal microscope where the focus of a laser is used to obtain the height of a structure. It is possible to scan a whole field of cross markers in several minutes. The obtained image is a greyscale image, where the greyscale corresponds to the height deviation of a structure. Therefore, both the crosses and the nanodiamonds appear in darker shades of grey. So in contrast to the previous method, information on the size and isolation of the nanodiamonds is accessible. After scanning the substrate with the laser scanning microscope, it is put into the confocal setup. While observing the surface with the CCD camera (Figure 1.5), a specific cross marker is chosen as the starting point of a fluorescence light scan. Comparing the laser scanning microscope image and a fluorescence light scan, fluorescent dots of the

specs

verify
info

fluorescence light scan are attributed to nanodiamonds in the laser scanning microscope scan (see Figures 1.21a and 1.21b).

===== »»> editing

1.1.3 The Pick-And-Place Process

The pick-and-place process aims to transfer a select nanodiamond between two substrates using the tip mounted inside a scanning electron microscopy. The advantage of using the SEM tip as a nanomanipulator lies in the fact that the progress of the manipulation process can be visualized directly, allowing for a better control of the operation. Figure 1.6 illustrates the process.

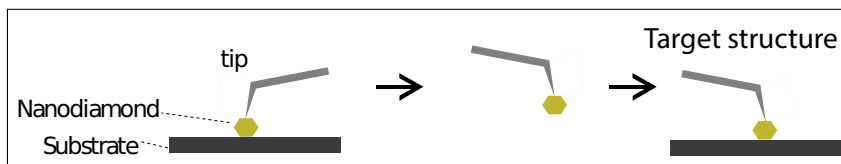


Figure 1.6: Sketch of the pick-and-place process

After we identified nanodiamonds as well-suited for transfer to the target structure, both the substrate with the nanodiamonds and the target structure were mounted inside the SEM. The process was performed using a high resolution mode with a low acceleration voltage of the SEM of 1 keV and a current of 1.7 nA. The tip is approaching the target pre-selected nanodiamond from above. As the SEM objective is mounted above the nanomanipulator, the proximity the nanomanipulator tip to the nanodiamond is not observable. To enable the tip of the nanomanipulator to pick up a target nanodiamond a precise approach is necessary. To facilitate this difficult procedure, the approach is divided into two stages: A coarse stage and a fine stage.

In the coarse stage the distance between tip and target nanodiamond is indirectly estimated from the shadow the tip itself casts onto the substrate and the focus area. As the tip approaches the target, the shadow of the tip starts to coincide with the nanodiamond position. At this point the fine stage of the approach begins in order to cover the remaining distance. To precisely control the final approach the focus of the SEM is used. Note that, as the distance between the tip and the target decreases, the focus must become sharp. Note that if the SEM is focused on the nanodiamond, the tip is out of focus and appears blurry. However, as the distance between the tip and the target decreases, the focus must become sharp. Thus the tip must be moved with utmost care until the focus becomes sharp at which point the tip touches the nanodiamond and pick-up can commence. While the process appears straightforward in concept, it is extremely challenging to operate the involved machinery to the required precision. As can be seen in Figure 1.2b it is easy to overshoot the target and to ruin the tip in the process.

When performed correctly, the nanodiamond sticks to the tip due to adhesion when the both get in contact, see Figure 1.7a. The nanomanipulator is then moved to the target structure and the approach procedure is applied in reverse. Figure 1.7b illustrates the tip of the nanomanipulator carrying a nanodiamond towards its destination structure. Depending on the material of the target structure, the nanodiamond either sticks to the structure right

away due to higher adhesion forces between the nanodiamond and the structure (as is the case for golden plasmonic antennas). Alternatively, a sideways motion of the nanomanipulator tip must be used in an attempt to strike-off the nanodiamond. Either way, with patience it is possible to place a nanodiamond in a target position within a precision of a few nanometers.

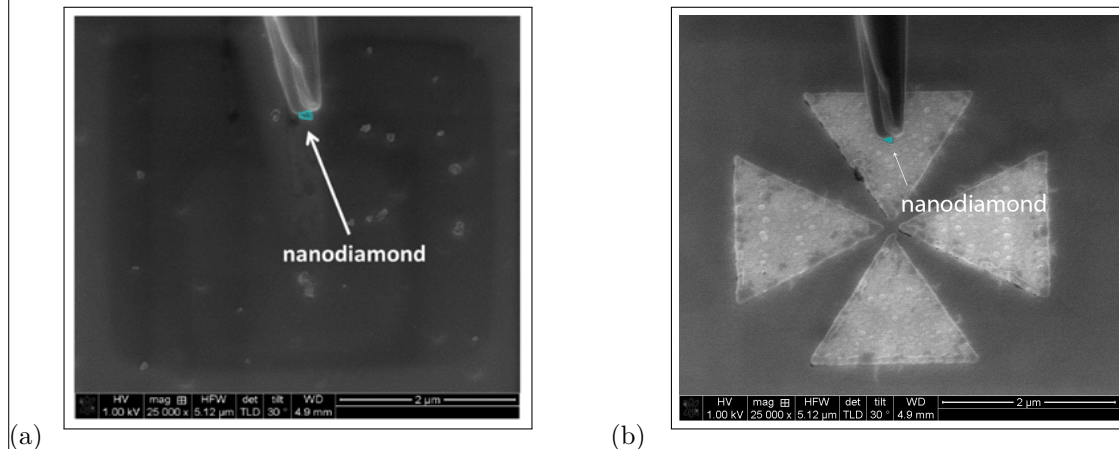


Figure 1.7: a) Tip of the nanomanipulator after successful pick-up of a nanodiamond. b) Tip of the loaded nanomanipulator approaching the target structure about to deliver a nanodiamond.

1.2 Coupling SiV centers to Vertical-Cavity Surface Emitting Lasers

For metrology, the photon flux rate has to be high enough to be measured by a low optical flux detector [?].

The red AlGaInP-based oxide-confined vertical-cavity surface emitting lasers (VCSEL) are compact and perfect candidates for excitation of SiV centers in a hybrid integrated single photon source: They exhibit wavelengths around 650 nm at continuous wave emission. SiV centers exhibit intensity maxima at an excitation at 670 nm and 690 nm []. In addition, VCSELs exhibit circular beam profile, have low divergence angle and emit linearly polarized light.

1.2.1 Vertical-Cavity Surface Emitting Laser Structure

The VCSEL structure (??) consists of an active region between two distributed Bragg reflectors (DBR). The bottom n-type DBR is made of 50 pairs of AlAs/Al_{0.5}Ga_{0.5}As, the p-type DBR consists of 36 Al_{0.95}Ga_{0.05}As/Al_{0.5}Ga_{0.5}As mirror pairs [?]. The active region consists of four GaInP quantum wells (QW). An oxide aperture in a field node of the standing wave serves as a spatial filter for maximum modal gain by confining the current and the optical mode. The active diameter which is defined by the oxide aperture amounts to 5.8 μm. As this region is the area where the laser emission exits the VCSEL, the nanodiamonds have to be put within this area. The used VCSEL exhibits an optical output power up to 1 mW with low threshold current of up to 3 mA at about 655 nm.

diagram
einfuegen

ist das
up to

nachdenke
wie for
mulierung
richtig
ist

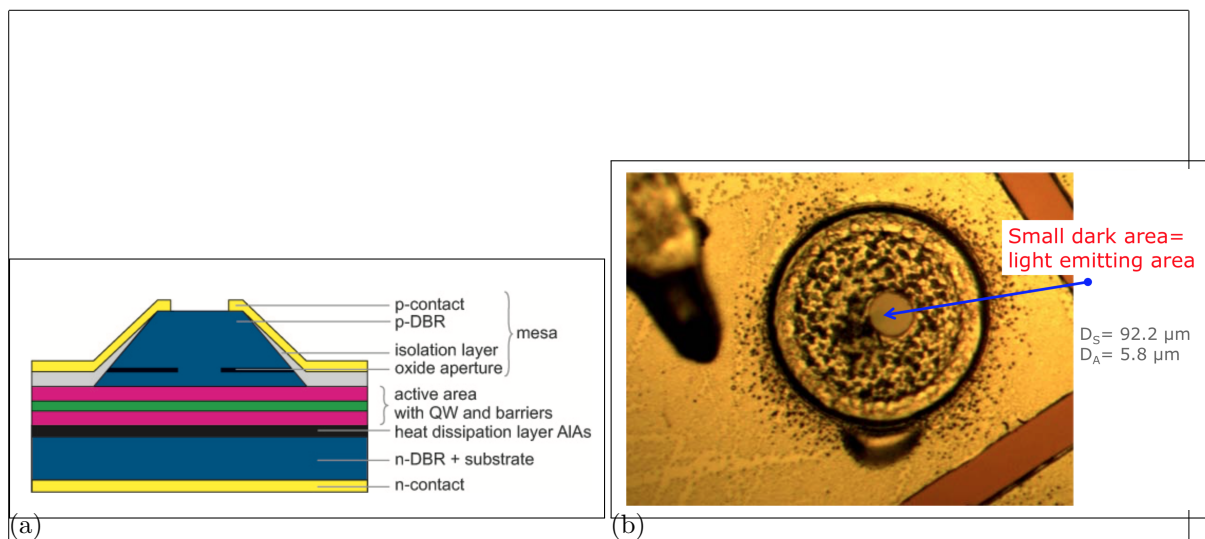


Figure 1.8: (a) Sketch of the VCSEL showing the different layers.

ask how to cite

(b) Image of the VCSEL. The circle with the black dots is the hole in the p-contact (diameter D_S , the smaller darker area in the middle is the laser output area (diameter D_A)

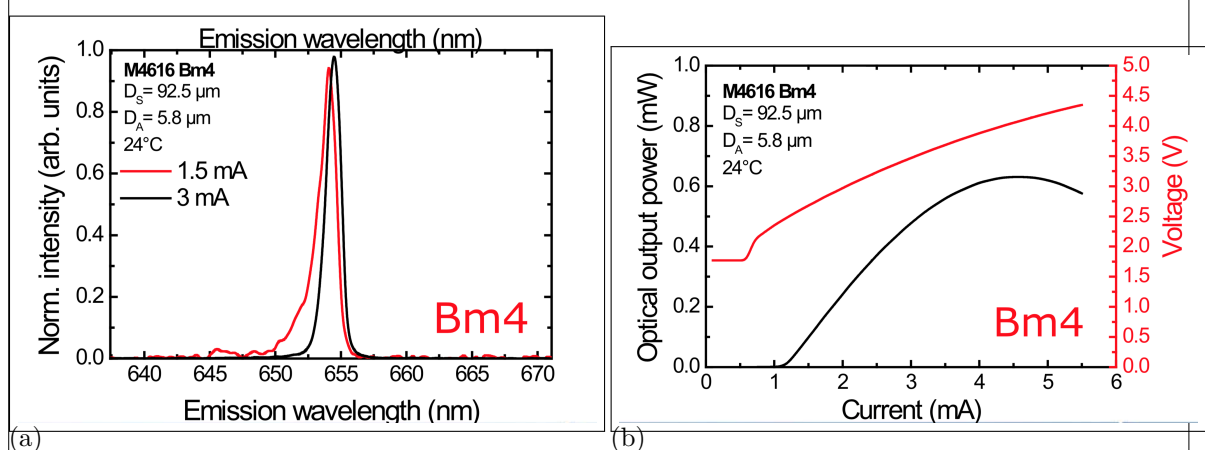


Figure 1.9: (a) Emission spectrum of the used VCSEL at two different currents. (b) Optical output power and voltage of the same VCSEL in dependence of input current. []

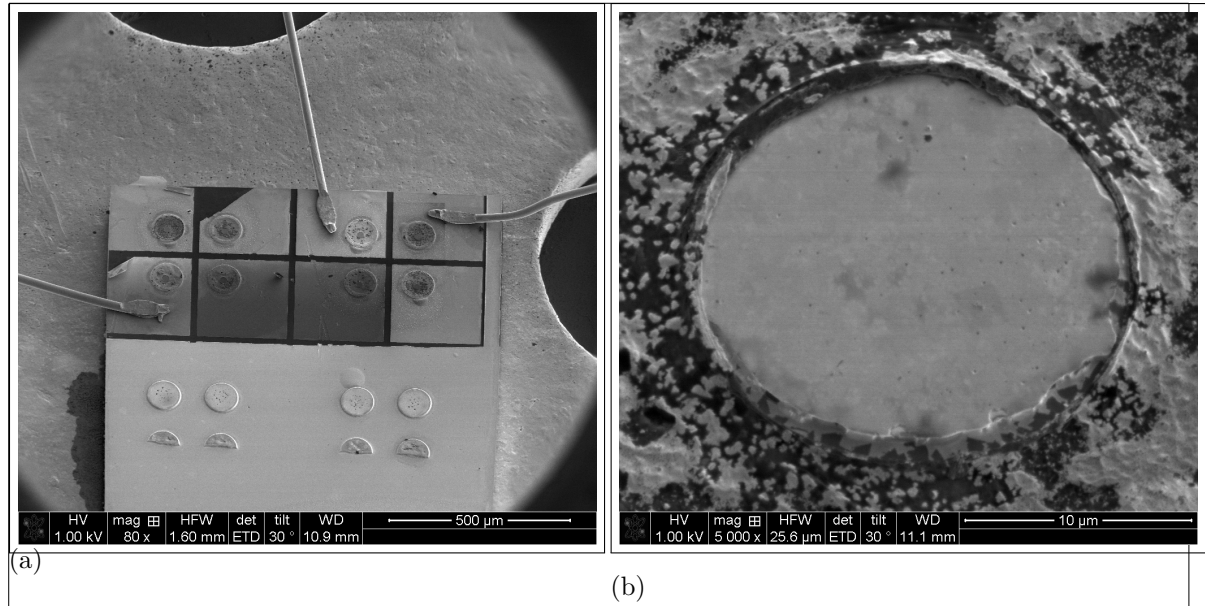


Figure 1.10: (a) SEM image of an array of VCSELs. The three wires are the anodes, which are connected to the top layer (p-contact) of the VCSEL. Therefore, three of the VCSEL structures can be operated. (b) Detail SEM image of the top of the exploited VCSEL Bm4. The circular middle part is the hole in the p-contact through which the top DBR is visible. The active diameter is smaller than that and not visible in the SEM.

1.2.2 SiV center in a Vertical-Cavity Surface Emitting Laser

As diamond material we used CVD grown nanodiamonds. They had been grown on an iridium coated silicon wafer (see ??). These nanodiamonds exhibit a nominal size of 200 nm. First, we selected a nanodiamond which exhibited one dominant line at 746.0 nm with a linewidth of 1.9 nm. Consecutively, its position on the substrate was determined using a white light laser scan as described in ?? . It was then transferred to the VCSEL Bm4 described in ?? . After a successful transfer of the pre-selected nanodiamond onto the active area of VCSEL Bm4, the VCSEL was put in the confocal setup. Using the laser from the confocal setup we checked if the pick-and-place process caused any modification of the spectroscopic properties of the SiV center such as a decrease of countrate or a modification of the fluorescence light spectrum. For this, the VCSEL itself was not operated itself. First, the VCSEL surface was scanned Figure 1.11a. A bright dot exhibiting a countrate of a few thousand counts per second is visible where the nanodiamond containing an SiV was put. A comparative scan of a VCSEL without nanodiamond only exhibits a background countrate, as expected (Figure 1.11b).

The spectrum of the SiV center in the transferred nanodiamond was investigated before and after the pick-and-place process (Figure 1.12). The original spectrum before nanodiamond transfer exhibits a sharp line at 746.0 nm (denoted line A). After the pick-and-place process, this line is still there, albeit with a low intensity. Another line at 0 nm (denoted line B) which was a minor feature in the spectrum before pick-and-place, is the predominant line after the process. This modification of the spectrum is caused by a reduction of the intensity of line A and constant intensity of line B. The reduction of the intensity of line A may be caused by damage of the color center due to electron radiation. While the energy of the electrons is low

was it
single?

check
number

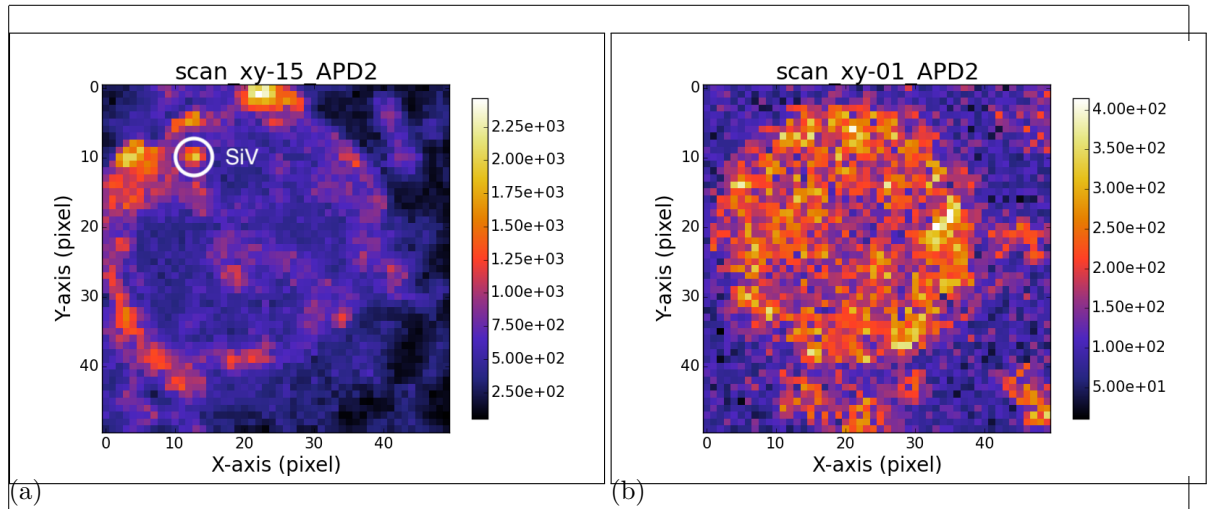


Figure 1.11: (a) Scan of the VCSEL Bm4 with coupled nanodiamond under excitation with the laser from the confocal setup. The big visible ring is the edge of the circular hole in the p-contact. The bright spot in the upper left corner corresponds to the transferred nanodiamond containing an SiV center. (b) Scan of the VCSEL Bm2 without nanodiamond under excitation with the laser from the confocal setup. The circular hole in the p-contact exhibits a constant countrate.

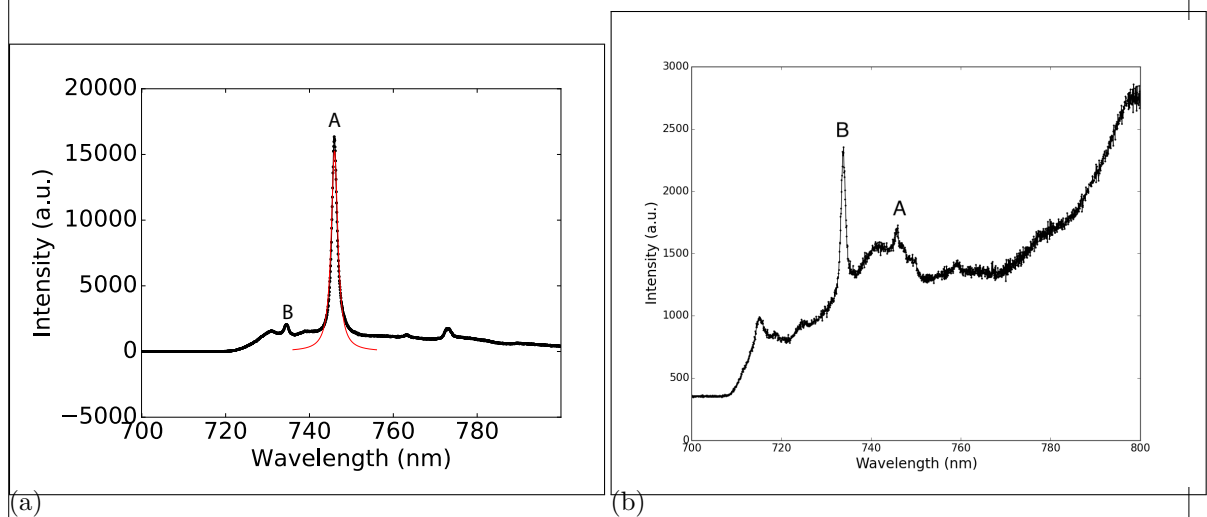


Figure 1.12: (a) Spectrum of the preselected diamond for transfer onto VCSEL Bm4 before pick-and-place. The strong line denoted A exhibits a center wavelength of 746.0 nm and a linewidth of 1.9 nm. Line B exhibits a center wavelength of 0 nm and a linewidth of 0 nm

put in correct numbers

(b) Spectrum of the same SiV center after pick-and-place, excited with the same laser as before. While Line A is almost gone, line B still exists and is the predominant line of the spectrum. Note: different longpass filters were used for the two measurements. Measurement (a) was performed with a 720 nm longpass filter, measurement (b) with a 710 nm longpass filter.

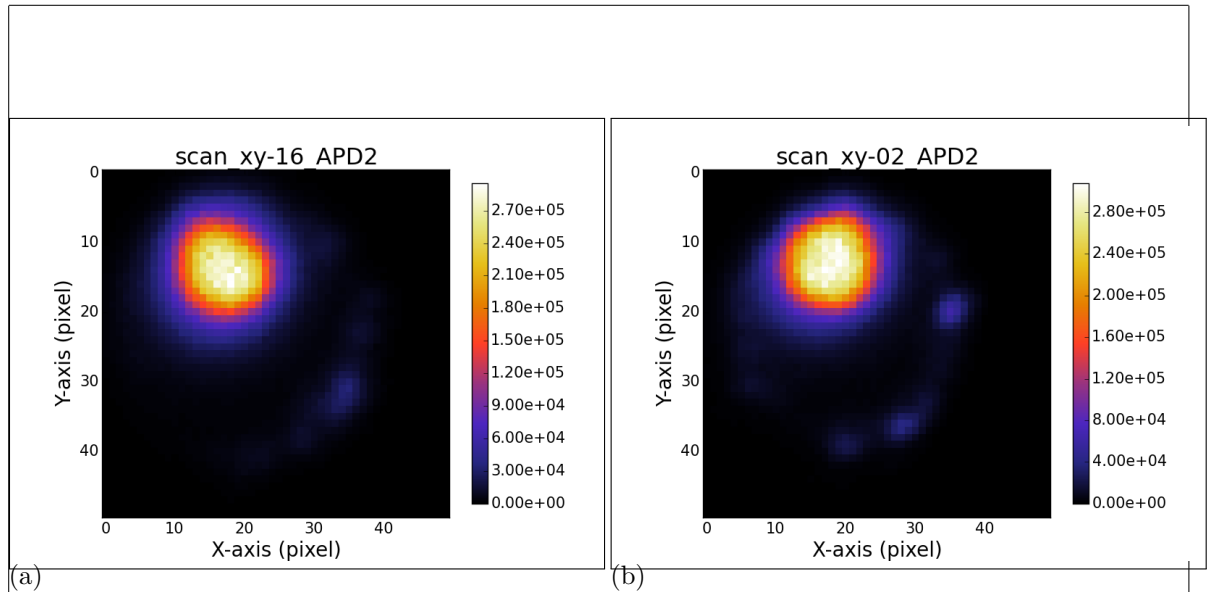


Figure 1.13: (a) Scan of the laser light stemming from the VCSEL Bm4 and the fluorescence light from the SiV center in the filter window 730 nm to 750 nm. (b) Scan of the laser light stemming from the VCSEL Bm2 without coupled SiV center. The outcome of the two scans is almost identical.

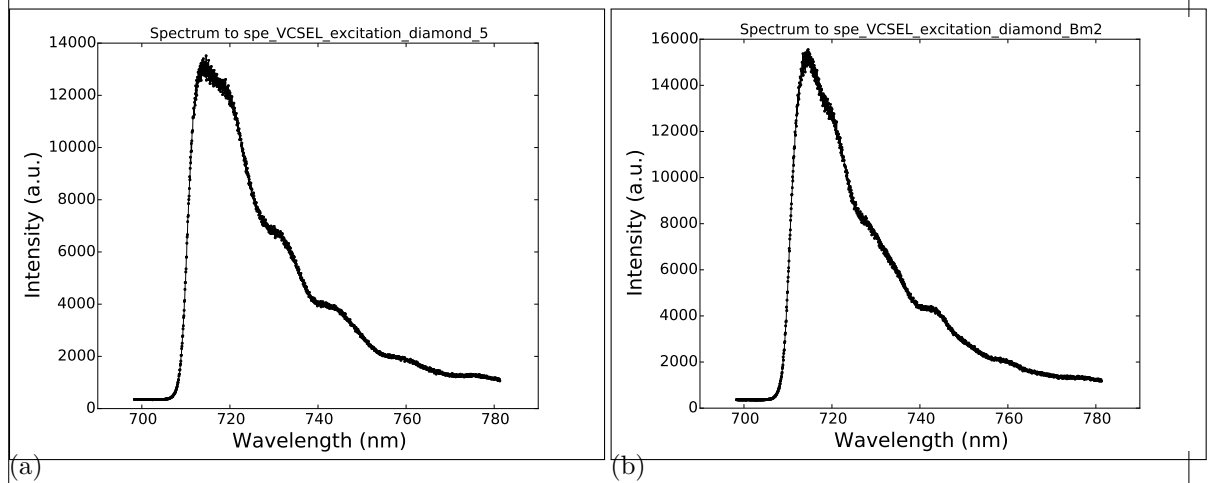


Figure 1.14: (a) Recorded Spectrum of the SiV center in the transferred nanodiamond on VCSEL Bm4 during VCSEL operation. No distinct SiV center lines are visible. (b) Recorded spectrum of VCSEL Bm2 (without SiV center)

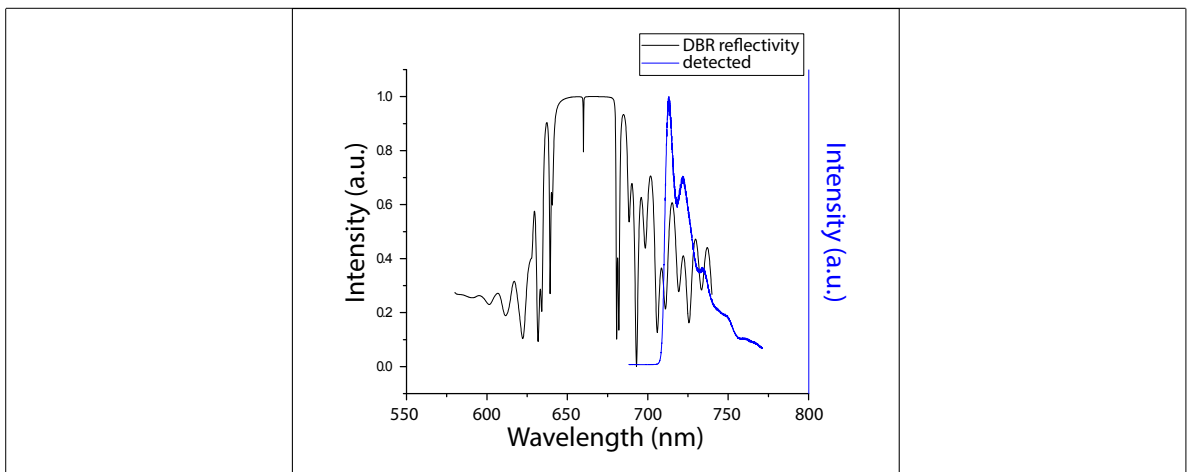


Figure 1.15: Reflectivity of the Distributed Bragg reflector (DBR) of the VCSEL, and spectrum of the SiV center measured during VCSEL excitation. The reflectivity of the DBR and the VCSEL emission spectra are depicted with different scales. The shape of the measurement of the SiV center during VCSEL operation coincides with the shape of the DBR reflectivity. The spectrum of the SiV center is not visible. As the emission from the SiV center is small compared to the intensity of the laser sideband in the same wavelength regime, the SiV centers emission is not detectable

warum schaut das spectrum anders aus als das, was einzeln geplottet ist?

compared to the ionization energy of the color center , we observed a reduction of fluorescence light intensity after electron radiation (for a detailed description of this effect, refer to [?]. We then operated the VCSEL at 0.84 mA and 3.3 V and turned off the laser of the confocal setup. We scanned both the surface of VCSEL Bm4 (with nanodiamond) and of VCSEL Bm2 (without nanodiamond) with a 730 nm to 750 nm bandpass filter. This filter window suppresses the VCSEL laser line at 655 nm (1.9a) while leaving the SiV center emission nearly unchanged. The light areas in Figure 1.13 correspond to the laser output areas. We measured a spectrum at the same points as before VCSEL operation. In the case of VCSEL Bm4, this spot corresponds to the position of the SiV center. The following observations are made from the measurements:

- In both scans, the laser output area is visible as a big bright spot. There is no difference in intensity between VCSEL Bm4 and Bm2.
- The spectra of VCSEL Bm4 and Bm2 are almost identical.

The spectrum recorded in the confocal setup corresponds well with the DBR reflectivity (Figure 1.15). Hence, we conclude, that the detected emission is due to the VCSEL and does not stem from the SiV center From these observations, we draw the conclusion that the fluorescence light emission from the SiV center is small compared to the sideband of the VCSEL emission in the wavelength regime where the SiV center emission is expected. Therefore, the SiV center emission is not detectable during VCSEL excitation.

Ongoing work is performed to reduce sideband emission of the VCSEL in the SiV center emission regime. A promising approach is to add a gold layer on top of the VCSEL which

numbers

besser
begruen-
den, was
passiert

ev besser
begruen-
den

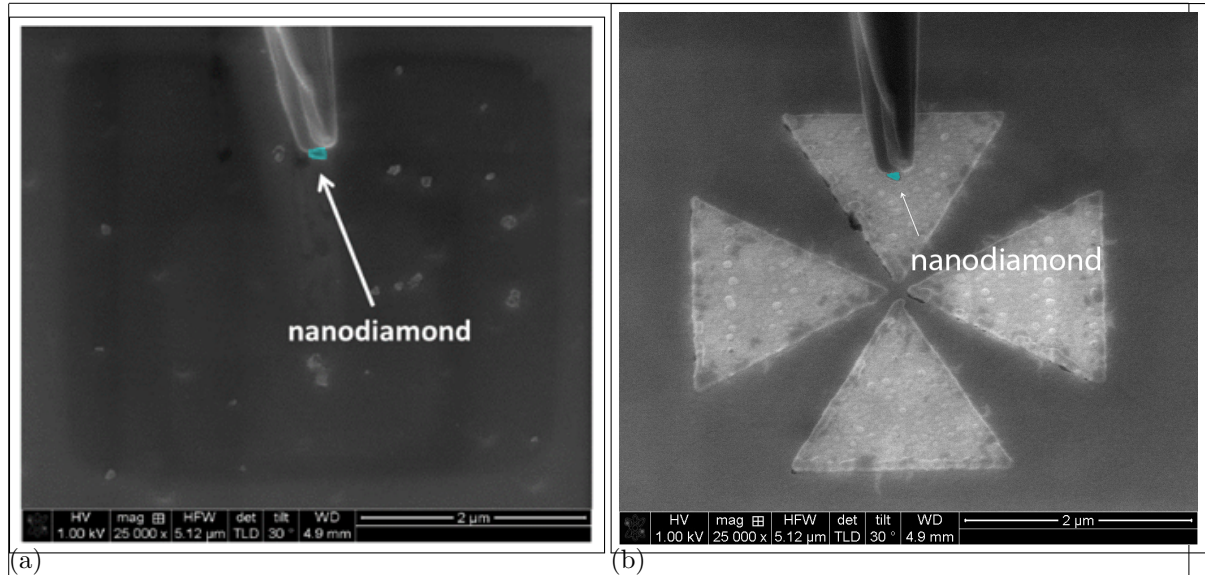


Figure 1.16: Pick and Place technique for nanodiamond manipulation, nanodiamond colored blue in the image for better visibility. (a) A nanodiamond sticking to the nanomanipulator tip which was lifted off the substrate (b) Transfer of the nanodiamond to the target antenna structure which is in the background.

acts as a tunable mirror. While films of gold have a transmittance maximum at 500 nm, the transmittance minimum depends on the film's thickness [?]. Hence the goal is to apply a gold film which suppresses the laser sideband in the SiV center emission regime.

In this chapter we showed successful transfer of a nanodiamond containing an SiV center. While the SiV center spectrum was modified after the pick-and-place process, it was clearly identified with the preselected SiV center. Further research has to be performed to enhance the VCSEL emission properties.

1.3 Coupling Nanodiamonds to Double Bowtie Antenna Structures

In this chapter, the integration of SiV centers in nanodiamonds with double bowtie nanoantenna structures is presented. The emission from the coupled system has two advantages:

- The antenna causes an enhancement in the SiV center's photoluminescence emission intensity.
- The photoluminescence spectrum of the nanodiamond is modified depending on the geometry of the nanoantenna as well as the position of the emitter in the gap. This provides the flexibility of designing the nanoantennas to accurately predict and tune the emitters' PL spectrum as desired.

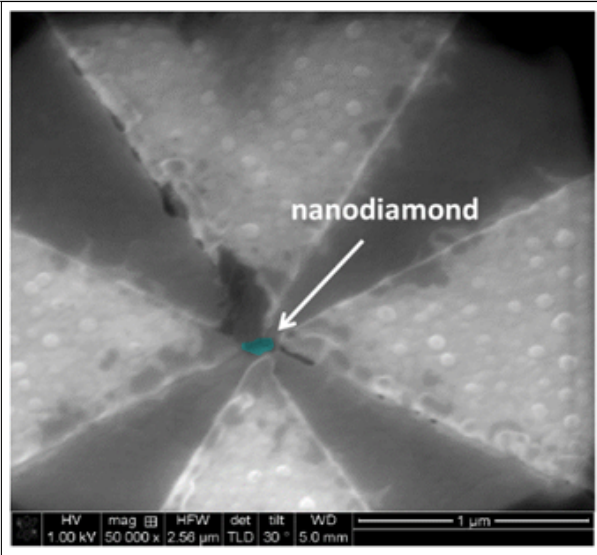


Figure 1.17: SEM detail image of the middle of the double bowtie antenna structure with the transferred nanodiamond. For better visibility, the nanodiamond is colored blue. Antenna damage caused by the placement of the nanodiamond is visible as black area at the tip of the top triangle

1.3.1 Plasmonic Antennas

nancy Doktorarbeit: Plasmons can be considered as a collective oscillation of the free electron density on the surface of a conducting material.

Localized surface plasmons (LSP) are the result of stationary resonant oscillations of the surface charge density at the boundaries of metallic nanostructures [37,38]. Due to their significant optical properties, LSPs are shown to enhance electromagnetic field confinement.

Plasmonic nanoantennas have proven to be very successful candidates in tailoring light propagation and confinement at the nanoscale. Electromagnetic antennas are defined as metallic devices used for receiving and transmitting electromagnetic waves. In addition to acting as probing devices, antennas must also serve as directional devices that optimize and accentuate radiation energy in some directions and suppress it in others [77]. Optical nanoantennas benefit from their sizes, which are comparable to or smaller than the wavelength of visible light, to overcome the diffraction limit and manipulate electromagnetic fields at the nanoscale [78]. This allows them to be widely used in many applications such as near-field optical microscopy [79], surface enhanced spectroscopy [80,81], sensing [82], medical therapy [83], and optoelectronic devices [84]. When light is incident on metallic nanoantennas, modes of standing waves are created at resonance. This creates an electric field enhancement in their vicinity. A good nanoantenna is characterized by its high collection efficiency (large cross section), and its ability to focus incident electromagnetic light into sub-wavelength areas (large near-field enhancement). To improve their performance, researchers have found that cutting a gap in the center of nanoantennas leads to a higher near-field enhancement while maintaining the same effective cross-section [85]. This occurs due to the coupling between the LSP modes of the two parts of the nanoantenna creating a hotspot in the gap. Exciting LSPs can be simply achieved by resonantly illuminating nanostructures with electromagnetic waves.

[?] Optical antennas, acting as converters between propagating and localized fields, provide

an effective route to couple photons in and out of nanoscale objects. These antennas are the counterparts of conventional radio and microwave antennas and operate in the visible regime (1, 2). Optical antennas have been shown to focus optical fields to subdiffraction-limited volumes (3), enhance the excitation and emission of quantum emitters (4–7), and modify their spectra (8).

A characteristic of antennas is their directed emission and reception. So far, the control of directionality has mainly been pursued by photonic crystal structures (9) and surface-plasmon-based devices (10–12). However, for such structures approaching the nanometer scale diffraction can limit the collimated beaming of light. On the other hand, the interaction of quantum emitters with light is best enhanced with microcavities (13, 14). Compared with these approaches, plasmonic nanoantennas offer a much smaller footprint in an open geometry combining strong subwavelength fields and increased transition rates, together with the prospect of directionality.

[?] from gold, a metal that can develop charge oscillations in its surface layers when excited by optical radiation. These antennas allow visible radiation, which has wavelengths of hundreds of nanometers, to couple into a semiconductor quantum dot only a few nanometers in diameter, and also direct the emission

Good mode-matched antennas reradiate their energy after excitation within a single cycle of the wave. Molecules or quantum dots take nanoseconds or even longer to reradiate their energy. This time scale corresponds to about 1 million oscillations at optical frequencies, and the emission is in all directions.

If an atom, molecule, or quantum dot is placed into the near-field of a metallic nanoantenna (within about 1/50th the wavelength of the emitted radiation), its excited state can radiate photons very efficiently to free space (see the figure, panel B). The quantum emitters can emit a single photon, which can be exploited in quantum optics. Additionally, the nanoantenna can redirect radiation into a defined solid angle in space and impose a specific polarization on it.

The demonstration of the Purcell effect, which is the acceleration of the decay of the quantum emitter caused by impedance matching by the antenna to free space, could also enhance the radiative emission over nonradiative losses

[?] The electro-magnetic antenna, originally referred to as an aerial, is a transducer between electromagnetic waves and electric currents, and generally operates in the radiofrequency regime. In analogy with the electro-magnetic antenna, we define the optical antenna as a device that converts freely propagating optical radiation into localized energy, and vice versa. The spatial extent of a receiver or transducer is commonly much smaller than the wavelength of radiation, λ , and is typically of the order of $\lambda/100$.

Surface plasmon resonances make optical antennas particularly efficient at selected frequencies. A generic antenna problem is illustrated in Fig. 3. It consists of a transmitter and a receiver, both represented by dipoles p . The antenna is introduced to enhance the transmission efficiency from the transmitter to the receiver. This enhancement can be achieved by increasing the total amount of radiation released by the transmitter, for which the antenna efficiency is a useful figure of merit:

$$\eta = \frac{P_{rad}}{P_{loss}} \quad (1.1)$$

where P is the total power dissipated by the antenna, P_{rad} is the radiated power and P_{loss} is the power dissipated through other means, such as by absorption in the antenna. However, the transmission efficiency can also be improved by directing the radiation in the direction of

the receiver. The efficiency for this process is represented by the directivity:

$$p = p \quad (1.2)$$

where the angles \hat{y} and \hat{T} represent the direction of observation and $p(\hat{y}, \hat{T})$ is the angular power density. The combination of antenna efficiency and directivity is referred to as the antenna gain:

$$p = p \quad (1.3)$$

By reciprocity, we can interchange the fields and sources in Fig. 3 to give $p_1 E_2 = p_2 E_1$, where E_1 (E_2) is the field of dipole p_1 (p_2) evaluated at the location of p_2 (p_1). A good transmitting antenna is therefore also a good receiving antenna. For a transmitter in the form of a two-state quantum emitter, reciprocity leads to a relationship between the emitter's excitation rate $\dot{\$}_{exc}$ and its spontaneous emission rate:

$$p = p \quad (1.4)$$

Here, the superscript abs refers to the absence of the antenna and the subscript \hat{y} indicates the polarization state; that is, the electric field vector points in direction of the \hat{y} unit vector. An equivalent equation holds for polarization in the \hat{T} direction. Interestingly, excitation in a direction of high directivity allows the excitation rate to be enhanced more strongly than the radiative rate. Another important antenna parameter is the antenna aperture, which is formally the same as the absorption cross-section sigma. Let us consider a dipole-like receiver with a cross-section $\dot{\$}_o$ that is not coupled to an antenna. The unit vector in the direction of the absorption dipole axis is denoted as n_p and the incident field at the location of the receiver is E_o . Once we couple the receiver to an antenna, the field at the receiver increases to E and the cross-section or antenna aperture becomes¹

$$p = p \quad (1.5)$$

Thus, the aperture of an optical antenna scales with the local intensity enhancement factor. Theoretical and experimental studies have shown that intensity enhancements of 10^4 – 10^6 are readily achievable^{14,36,37} and hence, for typical molecules with free-space cross-sections of $\sigma_{abs} = 1 \text{ nm}^2$, we find that a layer of molecules spaced $0.1\text{--}1 \mu\text{m}$ apart can absorb all of the incident radiation if each molecule is coupled to an optical antenna. Of course, this estimate ignores the coupling between antennas and therefore has limited validity.

1.3.2 Plasmonic Antenna Design

FDTD numerical simulations were performed using Lumerical software to characterize gold double bowtie nanoantennas on a gold substrate. The nanoantennas are tailored to have a gap of $g = 150 \text{ nm}$ (taking into account the diameter of the nanodiamonds of around 100 nm), side length of $L = 2 \mu\text{m}$, and a thickness of $t = 60 \text{ nm}$ (see Fig. 3a). Upon excitation with incident light, an intense electromagnetic hotspot is formed in the nanoantenna gap [?], which is expected to excite a nanodiamond containing SIV centers aiming to enhance its fluorescence emission. Unlike a single bowtie that is sensitive only to the polarization along its principle axis (C₂ rotational symmetry), a double bowtie features a C₄ rotational symmetry and therefore focuses both parallel and perpendicular polarizations (i.e. all in-plane directions). The index of refraction of gold is taken from Palik [?], and that of the nanodiamond is chosen

read paper

Palik, E. D. Handbook of optical constants of solids. 3, (Academic

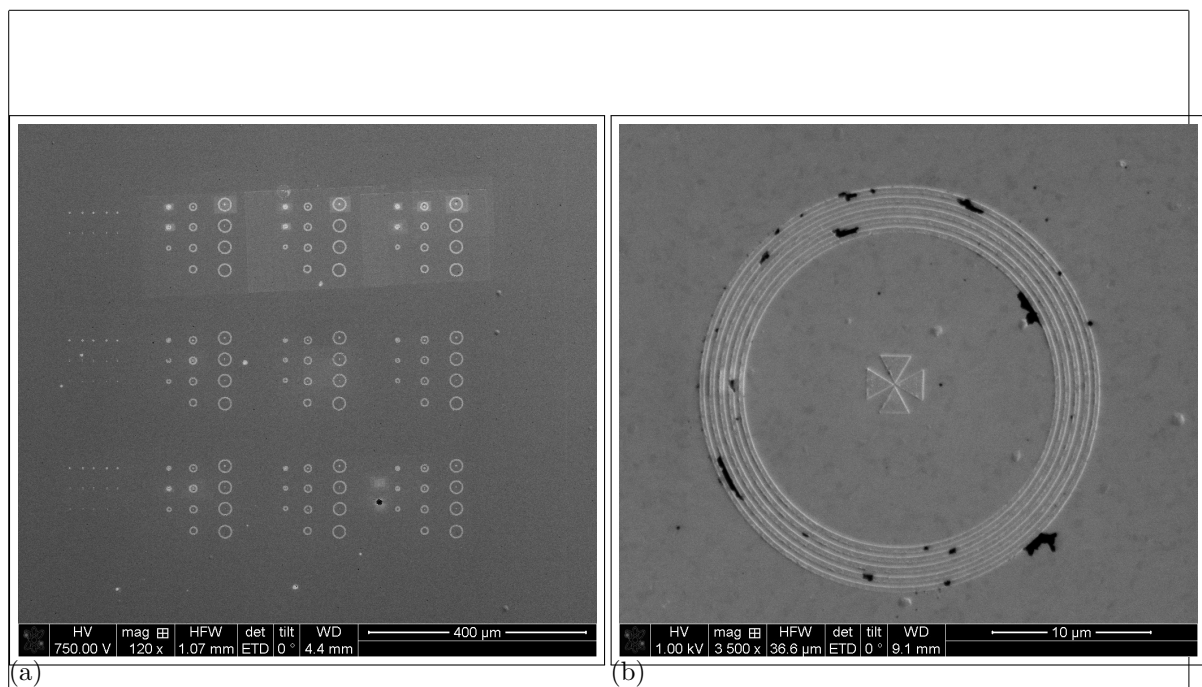


Figure 1.18: SEM images of the antenna structures. (a) Overview of a field of antenna structures exhibiting various dimensions. (b) Detail of one antenna structure. In the middle the double bowtie design is visible. The ring grating structure is surrounding it.

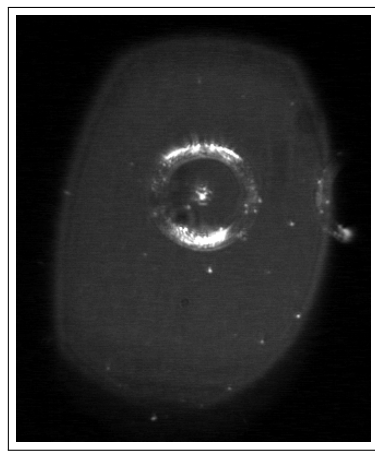


Figure 1.19: CCD image recorded in the confocal setup of an antenna structure under white light illumination. In the middle, the nanodiamond containing multiple SiV centers had been placed.

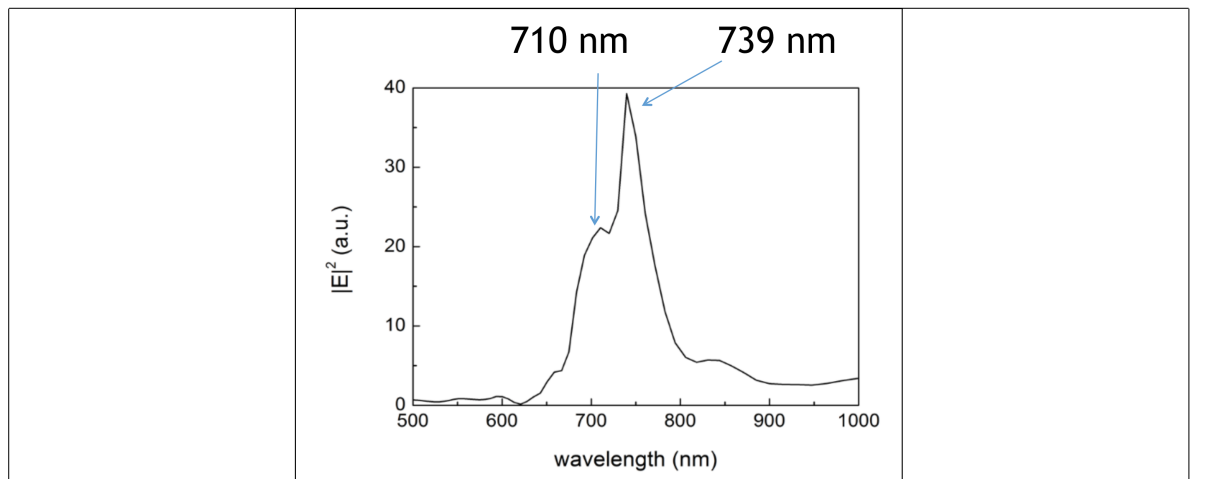


Figure 1.20: FDTD calculations of the electric field intensity as a function of wavelength in the gap of a double bowtie nanoantenna containing a nanodiamond.

to be $n = 2.4$ at $\lambda = 660$ nm. The electric field intensity in the nanoantenna gap is then measured as a function of wavelength to identify the antenna resonance. The spectrum is given in Figure 1.20 where we observe that the resonance shows two peaks; an intense peak coinciding with the SiV emission wavelength ($\lambda = 739$ nm), and an additional mode at a lower wavelength ($\lambda = 710$ nm) [?]. The resonance spectrum of the antenna alone shows only one peak at 739 nm. Thus, the additional peak is attributed to the presence of the nanodiamond that is slightly shifted from the center of the gap, corresponding to our experimental conditions. These calculations suggest, that the emission from an SiV center at 738 nm is effectively enhanced and directed by the antenna.

High optical confinement can be reached via successful SPP-LSP coupling at the nanoscale. One way of achieving that is by integrating diffraction gratings with nanoscale apertures or nanoantennas. Nanoantennas have shown to be very good candidates for focusing and enhancing electromagnetic fields in their vicinity. Nevertheless, due to their small size, a significant amount of the incident light is lost either by being scattered, reflected, or not entirely focused on the nanoantenna. On the other hand, plasmonic gratings act as sources for launching and orienting SPPs in a specific desired direction. Integrating a nanoantenna in the center of a concentric plasmonic ring grating creates a highly focused electromagnetic field at its center leading to an increase in the radiative decay rate as well as a collimated radiation of a dipole emitter placed inside [nancy::238–240] aus Nancys Doktorarbeit al ERlaerung, warum die antenne ringe herum hat Optical plasmonic focusing has been extensively studied in the field of nanoplasmonics and has very important applications in high resolution imaging, sensing, waveguiding, nanolithography, and sub-wavelength optics. For this purpose, researchers have investigated several plasmonic structures capable of enhancing and confining surface plasmons into sub-wavelength dimensions. Cavities composed of diffraction gratings acting as SPP launchers can be used as efficient nanoscale focusing devices [243,244], confined surface plasmon polariton amplifiers [245], and fluorescence emission enhancement tools [246] (Fig. 4.1a). It has been shown that the plasmonic AlJ_{Bull}-Eye structure, made of periodic concentric grooves in a metallic substrate, can lead to a strongly enhanced evanescent field focused in its center where propagating surface plasmons constructively interfere [247]. Controlling the directionality of transmitted light through an

fehlt
Erk-
laerung
zu Rin-
gen

aperture surrounded by periodic corrugations was also achieved, which allows overcoming the limitations of low transmittance and high diffraction in the sub-wavelength regime [248]. In a similar study, the aperture is replaced by a narrow slit in the center of the BullâŽs Eye antenna leading to a higher power coupling, narrower radiated beam, and good return losses [249]. In addition, ring grating structures can be used to control the luminescence directivity of emitters placed in the center. Fluorescence beaming of molecules placed in a nanoaperture surrounded by concentric metallic grooves was studied by directing their emission in a precise direction and with a specific angular width depending on their wavelength [250]. Similar work related to the fluorescence emission of quantum dots placed in a slit surrounded by a ring grating shows that their emission can be manipulated to form perfectly narrow collimated beams [251] (Fig. 4.1b). Ring gratings surrounding diamond nanoposts [186] and circular diamond nanowires [135] with embedded nitrogen-vacancy (NV) centers were also used to improve the collection efficiency and radiative decay rate of single NV centers. Directing the far-field emission of single NV centers placed in the center of a BullâŽs Eye grating was also recently investigated in a study that resulted in a high collection efficiency within a low numerical aperture [252]. This motivates us to use the ring grating structure described below to study efficient plasmon-emitter coupling at the nanoscale. An interesting property of the device is that the position of excitation determines the direction of propagation of the SPPs, providing a flexible mean of studying their interactions with molecules or dipole-like emitters placed on the surface.

1.3.3 SiV center in a Plasmonic Double Bowtie Antenna

In the following, specific details and challenges concerning the coupling process are given and results of the spectroscopic measurements of an SiV center in a plasmonic double bowtie antenna are reported.

We performed coupling the nanodiamonds containing SiV centers in two approaches: First we chose a nanodiamond containing several SiV centers for pick-and-place and afterwards a nanodiamond containing a single SiV center. As mentioned before, single SiV centers may be damaged by the electron radiation in the SEM during pick-and-place and stop emitting photoluminescence light. Hence, we decided to run first experiments with nanodiamonds containing multiple SiV centers. This approach has the advantages that we are able to gain experience in the execution of the pick-and-place process without the risk of permanently damaging the emitter and therefore rendering the tedious pick-and-place process futile. For measurements of the intensity enhancement by the antenna, a single emitter is necessary. However, the antenna's influence on the SiV center spectrum can be studied when several emitters are present. Therefore, studies of the spectrum are performed in this first approach.

After we gained experience with the first approach, we searched for a suited nanodiamond containing a single SiV center. The aim was to perform saturation and second order correlation measurements to probe single SiV centers, and consequently quantify the exact Purcell enhancement imposed by the nanoantenna on a single photon emitter.

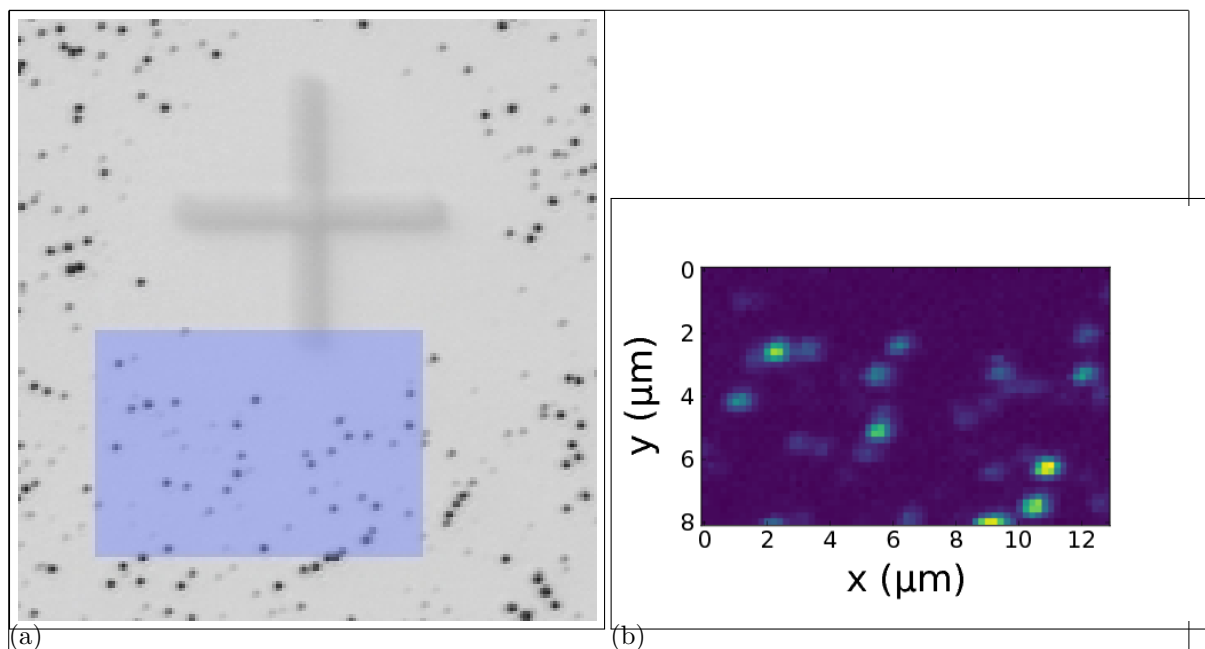


Figure 1.21: (a) Picture recorded with a commercial high resolution laser scanning microscope. The area shaded in blue represents the photoluminescence scan in image (b). (b) Photoluminescence scan of a $8 \mu\text{m} \times 13 \mu\text{m}$

Nanodiamond With Multiple SiV centers Coupled to Antenna

The nanodiamonds exploited for the approach of coupling multiple SiV centers to an antenna were produced by a wet-milling process from a CVD diamond film¹. The solution of nanodiamonds which exhibit a median size of 100 nm were spin-coated on an iridium substrate treated with Piranha etch. To ensure that a pre-characterized nanodiamond exhibiting preferred optical properties (eg. narrow linewidth, high count rate) is later found again, the iridium substrate was engraved with reference cross markers produced by a focused ion beam prior to the spin-coating process. After spin-coating, the sample was placed in an oven for 3 hours at 450 °C to oxidize the surface and remove any residual graphite and amorphous carbon.

Figure 1.24a shows the spectrum recorded of the preselected nanodiamond. The ZPL peak exhibits a wavelength of 738.55(1) nm and a linewidth of 5.00(3) nm. These numbers correspond well to the ZPL of unstrained SiV centers and therefore allows us to deduce that the studied nanodiamond contains at least one SiV center. Photon autocorrelation measurements revealed, that the nanodiamond contains multiple SiV centers.

To determine the position of the nanodiamond on the original substrate, first a scan with a commercial laser scanning microscope (LSM) was performed as described in ?? . ?? shows a part of an obtained LSM image. The cross marker can easily be identified, the black dots are nanodiamonds. After transferring the sample into the confocal setup, confocal scans of the corresponding areas are performed (Figure 1.21b). The area corresponding to the fluorescence light scan in Figure 1.21b is shaded blue in Figure 1.21a. When looking closely,

¹wet-milling performed by A. Muzha, group of A. Krueger, Julius-Maximilians Universität Würzburg, diamond film grown by group of O. Williams, School of Engineering, Cardiff University

fehlergrenzen
verfünen
machen

the bright spots in the fluorescence light scan can be identified with nanodiamonds visible in Figure 1.21a. The image in the SEM is very similar to the image obtained by the LSM. Therefore, once a nanodiamond containing a preselected emitter is identified in the LSM scan, it is easy to find the same emitter in the SEM.

The picking part of the pick-and-place process was performed in the same manner as described in the section about VCSELs (??). The gold surface of the plasmonic antenna caused a high adhesion between the antenna surface and the nanodiamond. Once the nanodiamond touched the gold, it could not be picked up again with the tungsten tip. The nanodiamond first touched the antenna structure a few nanometers away from the gap and immediately stucked to the surface, on top of one of the triangles. Therefore, the nanodiamond had to be pushed into the gap with the nanomanipulator tip. This process caused some damage to the antenna structure. The damage is visible as black area at the tip of the top triangle in Figure 1.17. However, FDTD simulations of damaged antennas reveal that this modification of the antenna hardly influences the antenna resonance.

After this deterministic placement, the antenna sample is placed in the confocal setup. The structure where the nanodiamond was placed is searched observing the sample surface in a CCD image under white light illumination (Figure 1.19). A scan of the antenna is performed in the confocal setup using the 660 nm continuous wave laser of the setup. The scan serves to locate the middle of the antenna structure and therefore the nanodiamond which had been placed there. An outline of the rings is visible in an overview scan of the antenna structure (Figure 1.23a). Zooming in to the middle of these rings, some of the edges of the bowtie antenna are vaguely visible (Figure 1.23b). This images suffices to approach the nanodiamond close enough to measure a PL spectrum. The PL spectrum of the SiV center in the nanodiamond gives insight to the effect of the nanoantenna on its emission. The result is displayed in Figure 1.24a. To rule out artifacts, a spectrum of an antenna of the same dimensions without nanodiamond is recorded (Figure 1.22b). The additional peak at a lower wavelength is attributed to the antenna resonance mode. To verify this, we convolute the experimental PL spectrum of the nanodiamond measured before placing it in the nanoantenna (??) with the intensity spectrum of the nanoantenna obtained by simulations (Figure 1.20). The resulting spectrum is given in Figure 1.24b, and is in good agreement with the measured spectrum in Figure 1.24a, confirming that indeed the extra peak is due to the antenna resonance.

bild dazu

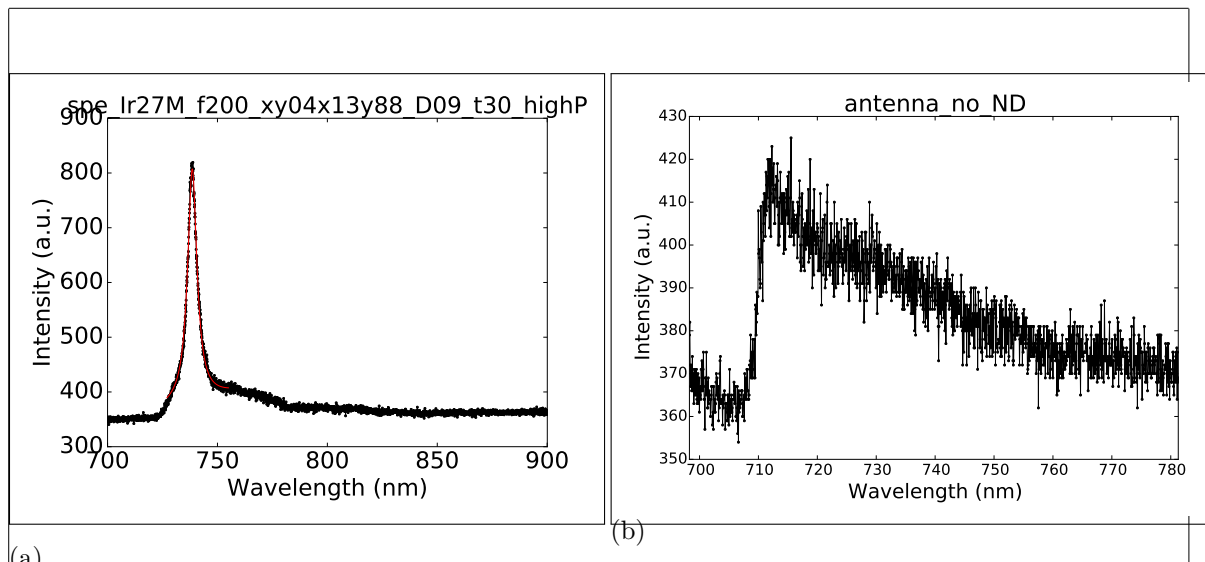
Nanodiamond With Few SiV center Coupled to Antenna

As the experiment of coupling a nanodiamond with an ensemble of SiV centers proved to be very successful, the next step was to select a nanodiamond with only few SiV centers, i.e. that it exhibits countrate saturation and a dip in the $g^{(2)}$ function. In this section, coupling a nanodiamond containing only few SiV centers to a double bowtie antenna is reported. It is an intermediate step between coupling. The origin sample used for this experiment is an iridium substrate onto which a solution of nanodiamonds were drop-casted. Starting material for the nanodiamonds was a electronic grade diamond film produced by the company rho-BeSt coating (now CarbonCompetence). It was then milled in a bead-assisted sonic disintegration process² to nanodiamonds of a size of . The nanodiamonds were drop-casted at 60 °C onto an iridium substrate containing cross markers which had been treated with Piranha etch. Preselecting a nanodiamond with a single SiV center is imposes additional constrains to the suitability of an nanodiamond if compared to a nanodiamond with multiple SiV centers. First,

checken,
ob
angaben
passen

groesse
einfuegen

²A. Krueger, Julius-Maximilians Universität Würzburg



(a)

(b)

Figure 1.22: (a) PL spectrum of the emitter in the preselected nanodiamond at room temperature. Black: experimental results; red: fit to experimental data,
verfuenftige fehlergrenzen einfuegen

which yields a ZPL center wavelength of 738.55(1) nm and a linewidth of 5.09(3) nm

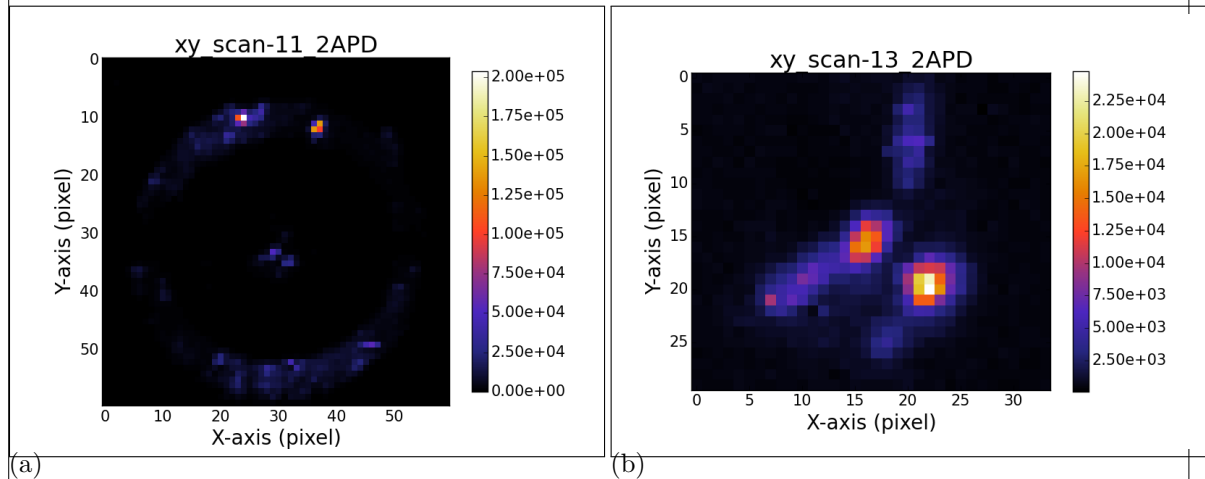


Figure 1.23: (a) Confocal scan of the double bowtie antenna where a nanodiamond containing multiple SiV centers had been placed. The rings are visible. (b) Detail scan of the triangles of the same antenna structure, which make up the double bowtie antenna. While the separate triangle cannot be seen, some edges and two bright spots are visible. To identify the place of the nanodiamond we compare the middle point of the rings in (a), the point of intersection of the edges and the bright spot and conclude that the upper bright spot in (b) is the location of the nanodiamond.

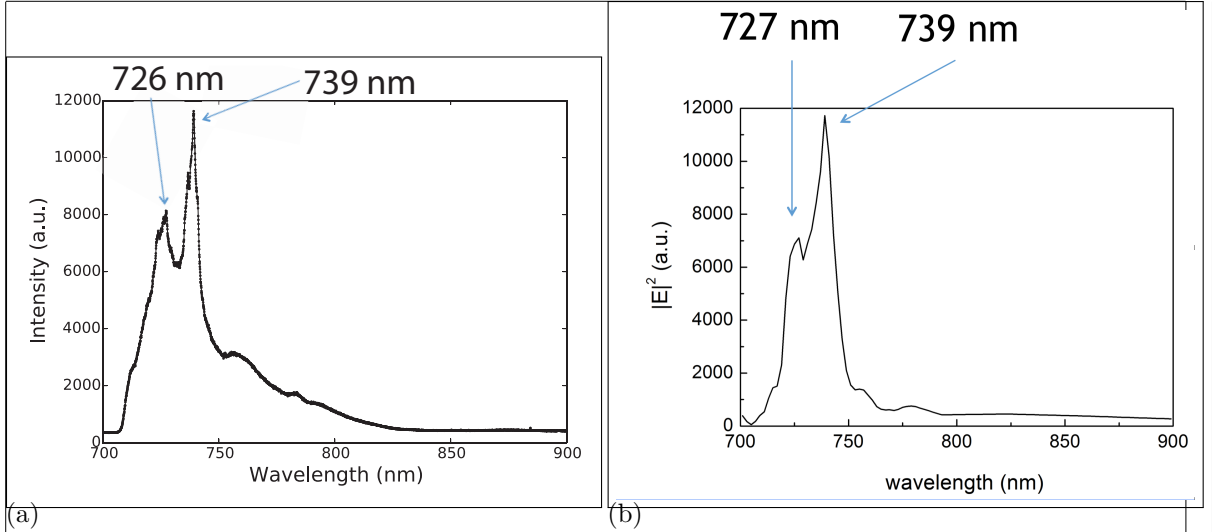


Figure 1.24: (a) Measured PL spectrum of the emitter after placing the nanodiamond into the nanoantenna, (b) Convolution of the spectrum of the measured PL spectrum of the emitter before pick-and-place (see Figure ??) and the simulated resonance spectrum of the nanoantenna (see Figure 1.20).

only a small percentage of the technically suited nanodiamonds (size, isolation) contain a single SiV center, second, damage due to electron radiation during pick-and-place. The position of the SiV centers on the substrate surface was performed in the same way as described in ???. The identification whether bright spots in the scan were suitable emitter was performed as follows: First a saturation curve was recorded. Countrate saturation is only a necessary and not a sufficient measure for single photon emission, hence the saturation measurement alone does not prove that the emitter in question is single. However, it takes only a few seconds to record a saturation measurement compared to potentially hour-long measurements of $g^{(2)}$ functions. Therefore, it is a quick selection method to evaluate potential candidates. Once an emitter with a saturating countrate was found, a spectrum was recorded to prove that the emitter in question is indeed an SiV center. At last, the $g^{(2)}$ function was recorded. We successfully found an SiV center with a small dip in the $g^{(2)}$ function. While the dip is too small to account for a single SiV center, it indicates the presence of only few SiV centers. Hence, we proceeded by transferring the host nanodiamond to the antenna structure.

The SiV center coupled to the antenna structure was then spectroscopically investigated in the confocal setup. First, we recorded a spectrum (spectrum A). The result of the first recorded spectrum revealed a multitude of peaks. To ensure that the peaks are no artifacts due to deficient alignment, we rechecked the alignment which proved to be precise. We initiated another measurement of the spectrum. However, this time the recorded spectrum only showed a broad background (spectrum B). After checking in the confocal scan that the measurement was performed at the correct position, we had to conclude that the emitter bleached shortly after recording spectrum A.

As mentioned earlier, the electron radiation may damage SiV centers in nanodiamonds. The electron radiation might have put the SiV center into an unstable state. Although we were still able to measure one spectrum, further application of energy from the laser seems to have permanently bleached the SiV center. While we cannot solidify this conclusion with further experimental evidence, we observed in earlier independent measurements that some

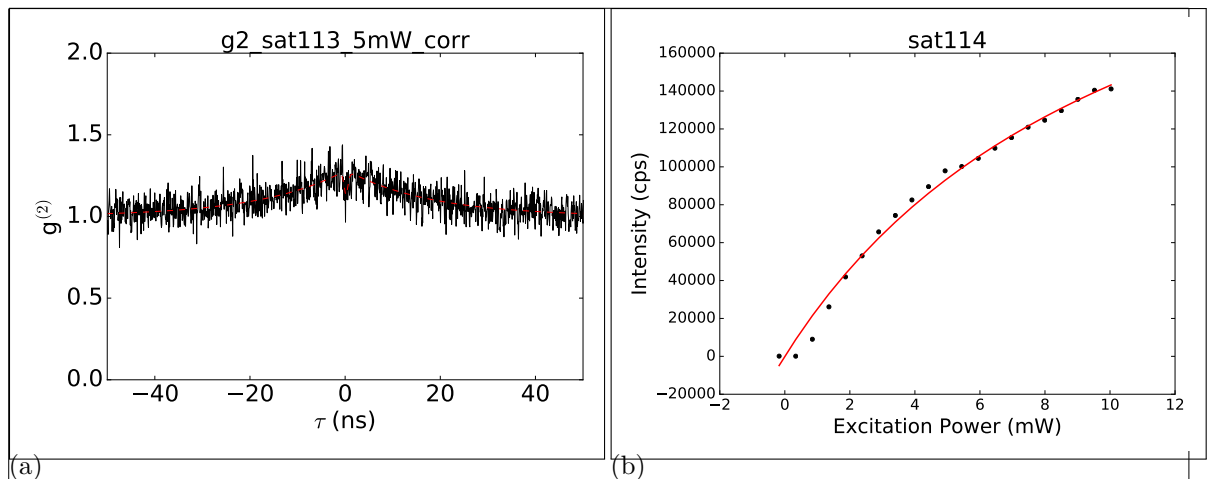


Figure 1.25: (a) The $g^{(2)}$ function of the preselected nanodiamond hosting few nanodiamonds. A dip at $g^{(2)}(0)$ is present, however it does not decrease below 0.5. While this indicates that more than one SiV center is present, a small number of SiV centers cause a dip in the $g^{(2)}$ function instead of no dip at all which would be measured under coherent emission

cps zu a.u. aendern

. (b) Saturation curve of the same emitter

zahlen fuer sat eintragen

. Data points are black, fitted curve red.

SiV centers bleach after electron radiation and that some SiV centers bleach after an extended laser irradiation [1]. The observations in this measurement suggest a combination of the two effects.

We performed FDTD calculations of the selected SiV center in the host nanodiamond in the plasmonic double bowtie antenna as described in the previous section. We used spectrum B to perform background correction of spectrum A and fitted the measured peaks (Figure 1.27b). In the simulations, we do not see the peaks between 700 nm to 750 nm that we recorded in the measurement. Hence, we conclude, that not additionally to the observed photobleaching, also the emitter's spectrum was modified in the pick-and-place process. While it is not possible to pinpoint exactly which circumstance caused the modification, possible candidates are.

To gain further insight, we performed FDTD calculations with antenna damage and different dipole orientation. To be able to include the dipole orientation into the calculations, a dipole emitter with a broad emission instead of a narrow emission peak has to be used. Therefore, the convolution method as described in the previous section is more adequate for our purpose, as the SiV center exhibits a very narrow emission peak. However, these calculations give further insight. First, the antenna damage does not have a big effect on the spectra, however the dipole orientation changes the results drastically (??). Therefore, future experiments should include polarization measurements to experimentally quantify the impact of the emitter orientation.

put in pictures

enter candidates and explain why

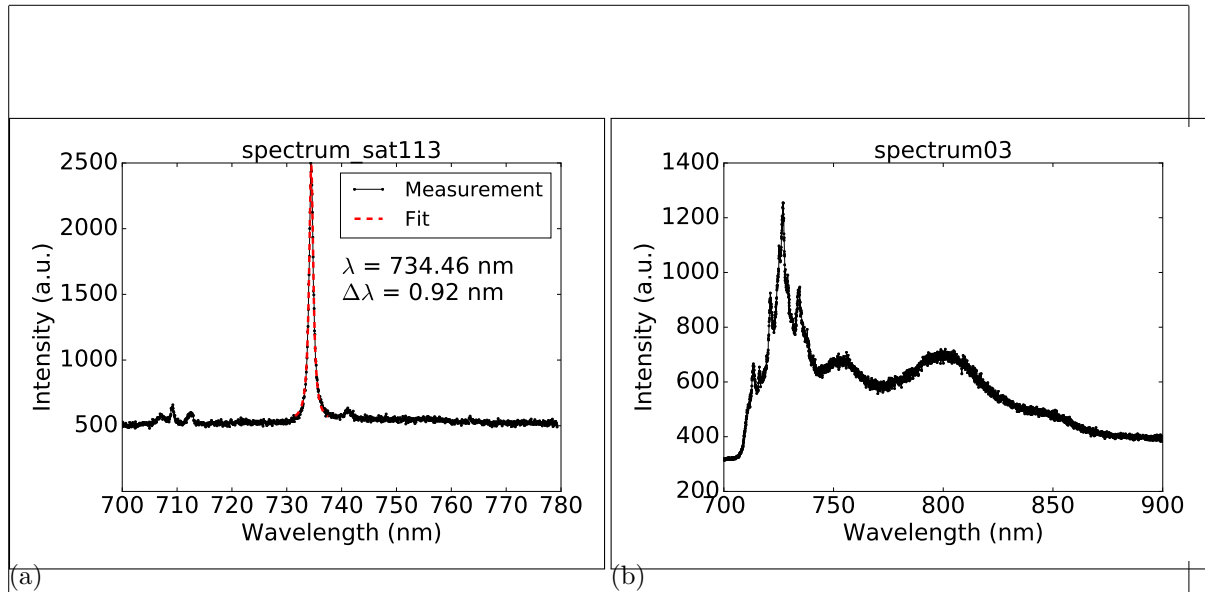


Figure 1.26: (a) Spectrum of the preselected nanodiamond hosting few SiV centers. (b) Measured spectrum after transfer of the preselected nanodiamond into the double bowtie antenna.

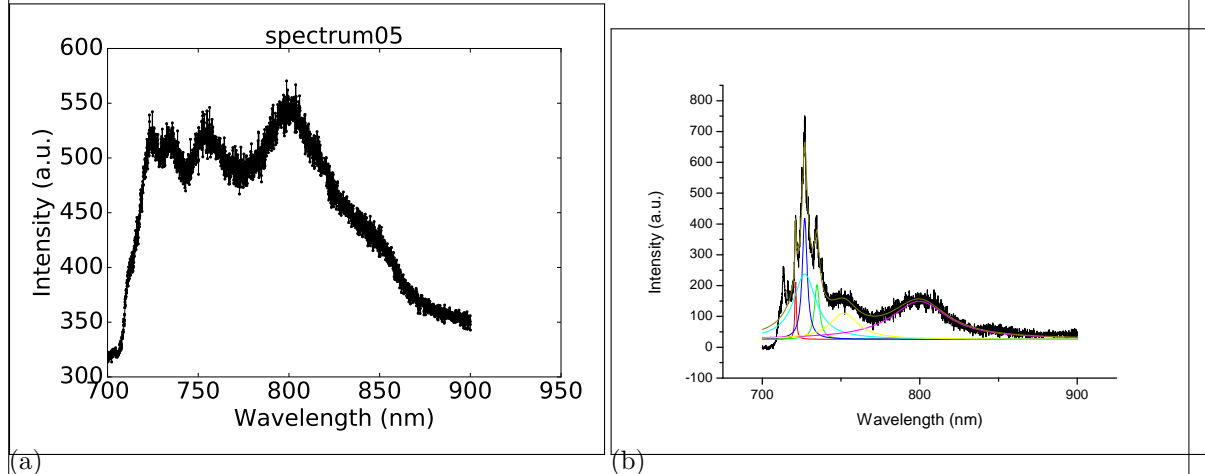


Figure 1.27: (a) Spectrum of the nanodiamond hosting few SiV centers coupled to the double bowtie antenna after the emitter bleached. (b) Background corrected spectrum of the transferred nanodiamond in the double bowtie antenna. Peaks are fitted, results of the fits are the colored lines. For background correction, the spectrum in (a) was used.

Outlook: Coupling a Nanodiamond With a Single SiV center to the Plasmonic Double Bowtie Antenna

To effectively state the emission enhancement of the SiV center by the plasmonic double bowtie antenna, a single SiV center is necessary. A correct measure for the emission enhancement is the saturation count rate. The saturation count rate is proportional to the inverse of the emitter's lifetime. Hence, if there are two or more emitters present, photons of the individual emitters are emitted randomly, which renders a correct saturation measurement impossible. However, finding SiV centers in nanodiamonds which fulfill both spectroscopic ($g^{(2)}(0) \approx 0$, saturation, narrow ZPL spectrum) and technical (size, isolation of nanodiamonds) constraints turned out to be a very time-consuming work.

We investigated different kinds of nanodiamonds in the search of nanodiamonds exhibiting optimal spectroscopic and technical parameters. We were able to fulfill the size requirements posed by the pick-and-place process and antenna design by producing different patches of different sizes of nanodiamonds and took the ones which were best suited. We also developed a good isolation of the nanodiamonds on the substrate by treating the iridium substrate with Piranha etch and tuning the amount of diamond solution drop-casted onto the substrate. This leaves us with the need of a higher probability of exactly one SiV center per nanodiamond. Parameters which have an impact on the quantity of SiV centers per nanodiamond are the initial SiV center density in the starting material and the nanodiamond size. Once the time constraint of finding a single SiV center in a nanodiamond is overcome, we can apply the extensive methods and knowledge gained by the reported procedures to couple a single SiV center to a plasmonic bowtie antenna.

To our knowledge, our experiments were the first time an SiV center in a nanodiamond was coupled to a plasmonic bowtie antenna. The extraordinarily precise correlation of the theoretically predicted and the experimentally recorded spectrum of an ensemble of SiV centers in a nanodiamond make this process a promising candidate for future applications.